Journal of Materials Chemistry

Dynamic Article Links

Cite this: J. Mater. Chem., 2012, 22, 19684

www.rsc.org/materials

PAPER

Calcium-based functionalization of carbon nanostructures for peptide immobilization in aqueous media

C. Cazorla,*[a] V. Rojas-Cervellera[bc] and C. Rovira[bcd]

Received 13th June 2012, Accepted 27th July 2012
DOI: 10.1039/c2jm33811d

We predict a covalent functionalization strategy for precise immobilization of peptides on carbon nanostructures immersed in water, based on atomistic first-principles simulations. The proposed strategy consists of straightforward decoration of the carbon nanosurfaces (CNS, *e.g.* graphene and nanotubes) with calcium atoms. This approach presents a series of improvements with respect to customary covalent CNS functionalization techniques: (i) intense and highly selective biomolecule–CNS interactions are accomplished while preserving atomic CNS periodicity, (ii) under ambient conditions calcium-decorated CNS and their interactions with biomolecules remain strongly attractive both in vacuum and aqueous environment, and (iii) calcium coatings already deplete the intrinsic hydrophobicity of CNS thus additional functionalization for CNS water miscibility is not required. The observed biomolecule–CNS binding enhancement can be explained in terms of large electronic transfers from calcium to the oxygen atoms in the carboxyl and side-chain groups of the peptide. The kind of electronic, structural and thermodynamic properties revealed in this work strongly suggest the potential of Ca-decorated CNS for applications in drug delivery and biomaterials engineering.

I. Introduction

Graphene (*i.e.* one-atom thick planar sheet of carbon atoms densely packed in a honeycomb crystal lattice) and carbon nanotubes (CNT, *i.e.* carbon allotropes of cylindrical shape with large length-to-diameter aspect ratio) are rigid low-dimensional systems with unique mechanical and electronic properties.[1,2] Recent progress in the synthesis and understanding of these carbon nanostructures (CNS) has revolutionized a number of modern scientific disciplines like biosensing, energy storage and harvesting, microelectronics, biomaterials modeling and drug delivery, to cite just a few.[3–8] Of particular relevance to the field of biotechnology is the immobilization of proteins and molecules on the surface of inorganic frameworks with nanometer resolution.[9–11] Typically, the interactions of biomolecules with pristine carbon nanostructures are long-ranged and very weak thus chemical modifications (functionalization) of the latter are required in order to enhance them. In addition, biomolecule–CNS forces in an aqueous environment generally turn out to be flawed due to the inherent hydrophobicity of CNS. Consequently, design of functionalization techniques for increase of CNS interactivity and solubility in water is of pivotal importance for biotechnological applications.

CNS functionalization techniques can be broadly classified as covalent and non-covalent. While chemical bonds between the nanostructure and biomolecule attractors are formed in covalent strategies, only interactions of the physisorption type are involved in the non-covalent approach (see Braet's Review[12] and references therein). In spite of the large number of studies focused on the immobilization of biomolecules on carbon nanostructures using non-covalent techniques,[13–17] better bond selectivity and thermodynamic stability can be achieved with covalent functionalization. Customary covalent functionalization techniques, however, mostly rely on oxidizing treatments inherited from the graphite chemistry like sonication in sulfuric and nitric acid, refluxing in nitric acid, ozonolysis, and air oxidization. In these treatments, abundant reactive defect sites are created on the carbon surfaces which are populated with carboxyl (*e.g.* RCOOH) and amine (*e.g.* RNH_2) functional groups acting as biomolecule traps.[18–21] Unfortunately, aggressive oxidizing functionalization techniques may incur unwanted changes on the physical and conformational properties of CNS so leading to unpredictable and/or inefficient performance of the resulting nanocomposites. Moreover, undesirable side reactions of intermolecular conjugation may also occur since most of the biomolecules are rich in RCOOH and RNH_2 species. Development of improved non-defecting and poorly interfering CNS functionalization techniques, therefore, is very desirable.

In the light of atomic first-principles simulations, we propose in this study a new covalent functionalization strategy for precise

[a]Institut de Ciència de Materials de Barcelona (ICMAB-CSIC), Campus UAB, 08193 Bellaterra, Spain. E-mail: ccazorla@icmab.es
[b]Computer Simulation and Modeling Laboratory (CoSMoLab), Parc Científic de Barcelona, 08028 Barcelona, Spain
[c]Institut de Química Teòrica i Computacional (IQTCUB), Parc Científic de Barcelona, 08028 Barcelona, Spain
[d]Institució Catalana de Recerca i Estudis Avançats (ICREA), 08019 Barcelona, Spain. E-mail: ccazorla@icmab.es

immobilization of peptides on CNS immersed in water. Our technique consists of straightforward decoration of the carbon surfaces with calcium atoms and, as it will be shown later, entails a series of advantages with respect to customary oxidizing approaches: (i) intense biomolecule–CNS interactions are accomplished while preserving atomic CNS periodicity, (ii) calcium-mediated organic-CNS forces are highly selective, hence allowing for prediction of general structural trends in the resulting nanocomposites, (iii) calcium-functionalized CNS and their interactions with biomolecules are stable under ambient conditions either in vacuum or aqueous media, and (iv) calcium coatings already promote the localization of water molecules close to the carbon surfaces so counteracting the intrinsic hydrophobicity of CNS. Furthermore, from a practical point of view Ca-functionalized CNS appear propitious for large-scale production, thanks to recent progress achieved in clean ion-implantation and arc discharge methods,[22,23] and the natural abundance of calcium. Besides this, calcium ions are already ubiquitous in living organisms so that Ca-functionalized CNS *a priori* seem to endorse a certain degree of biocompatibility.

The computational techniques employed in this study accurately reproduce the electronic structure of organic-CNS systems at the *ab initio* level, that is, without relying on interatomic bond assumptions. Consequently, the computational workload associated with the simulations is huge. For this reason, and since we are mainly interested in identifying the fine details of Ca-mediated biomolecule–CNS interactions, we adopted a peptide chain model to represent the organic component in nanohybrid systems. The peptide is composed of glycine (Gly, NH_2–CH_2–COOH), proline (Pro, NH–C_4H_7–COOH) and hydroxyproline (Hyp, NH–C_4H_6(OH)–COOH) amino acids (henceforth referred to as Gly–Pro–Hyp or peptide). Such a system has the repeating pattern of the sequence of collagen, the main component of connective tissue and the most abundant protein in mammals, thus is expected to capture the chemistry of collagen–CNS interactions.[24] Regarding the modeling of inorganic frameworks, we have considered both flat graphene and curved (n, 0) zig-zag nanotubes with radii ranging $2.4 \leq R_{CNT} \leq 6.0$ Å. (A comprehensive study of the energetic and structural properties of Ca-decorated CNS can be found in ref. 25; see also ref. 26–30.) Also, we have investigated the potential of bulk calcium graphite (CaC_6), a well-known graphitic intercalate material that can be routinely synthesized in the laboratory,[31,32] as a biomaterial component.

This article is organized as follows. In Section II, we describe in detail the models and methodology employed. In the next section, we present our results for the binding energy, structural properties, and thermal stability of hybrid peptide–Ca@CNS systems in vacuum and aqueous media. Also in Section III, we explain the electronic structure mechanisms behind Ca-mediated organic–inorganic interactions. Finally, we summarize the main results and present the conclusions in Section IV.

II. Computational methods and systems description

Density functional theory (DFT) calculations were performed using the projector augmented wave scheme due to Blöchl[33] and as implemented in the VASP code.[34] The exchange-correlation energy in the Kohn–Sham equations was approximated with the generalized gradient functional described by Perdew–Burke–Ernzerhof.[35] All energy cut-offs were set to 400 eV and the electronic states $2s^2\,2p^2$ of C, $2s^2\,p^3$ of N, $2s^2\,2p^4$ of O, and $3p^6\,4s^2$ of Ca atoms were considered in valence. (The adequacy of this approach at describing the interactions of small amino acids with CNS has been recently demonstrated in ref. 36.)

Atomic geometry relaxations were performed using a conjugate-gradient algorithm that kept the volume and shape of the unit cell fixed.[37] Peptide binding energies were calculated with the formula:

$$E_{bind} = E_{Hyb} - (E_{Ca@CNS} + E_{peptide}), \quad (1)$$

where E_{Hyb} stands for the energy of the fully geometry optimized peptide–Ca@CNS system and the rest of the terms for the energy of the individually relaxed Ca-decorated CNS (Ca@CNS) and peptide units. According to this definition, and ignoring thermal effects, negative E_{bind} values correspond to energetically favorable peptide binding. An atomic force tolerance of 0.02 eV $Å^{-1}$ and a special Monkhorst–Pack[38] k-point grid of $2 \times 2 \times 2$ were imposed in all the geometry optimizations. (We checked that by using these parameters total energy values were converged to less than 5 meV per atom.) In order to generate the initial peptide–Ca@CNS configurations, we first geometry optimized the peptide and Ca@CNS systems individually (see Fig. 1) and then joined them with a relative separation of ~4 Å between their centers of mass. For each system, we considered at least four different initial peptide–Ca@CNS orientations in which the number of oxygen or nitrogen atoms directed towards the Ca@CNS surface was maximized or minimized. Periodic boundary conditions were applied along the three box-edge directions, and the size of the simulation box was chosen so as to avoid spurious forces among neighbouring peptide replicas. In our slab-geometry CaC_6 simulations, we set a dipole correction in vacuum to compensate for the artificial electrostatic field derived from the imposed periodic boundary conditions.[39] We performed charge-density distribution (CDD) analysis based on the Bader theory[40,41] to quantitatively describe electronic charge transfers between atoms in the nanohybrids. In this framework, atomic charges are calculated by integrating the electronic charge density within regions of the space that are bound by electronic charge density minima. Electronic charge transfers quoted in this work correspond to atomic charge differences computed among the resulting joint systems and isolated integrating parts.

As noted in the Introduction, the organic component of the systems considered was modeled with a peptide chain composed of glycine (Gly), proline (Pro) and hydroxyproline (Hyp) amino acids joined by two peptide bonds (*e.g.* Gly–Pro–Hyp, see Fig. 1a). Hereafter we use the following notation to refer to the functional groups of the Gly–Pro–Hyp peptide: NH_2 for the terminal amine group, COOH for the terminal carboxyl group, CO for the carbonyl of the Gly–Pro bond, and COII for the carbonyl of the Pro–Hyp bond (see Fig. 1a). Regarding inorganic CNS, pristine graphene and zig-zag (n, 0) carbon nanotubes were modeled with a total of 54 and $96 \leq N \leq 180$ C atoms (depending on CNT radius), respectively (see Fig. 1b and c). Ca@CNS configurations were taken from ref. 25, where Cazorla *et al.* already determined the equilibrium structures as a function of calcium concentration, X_{Ca} (defined as the ratio of Ca to C

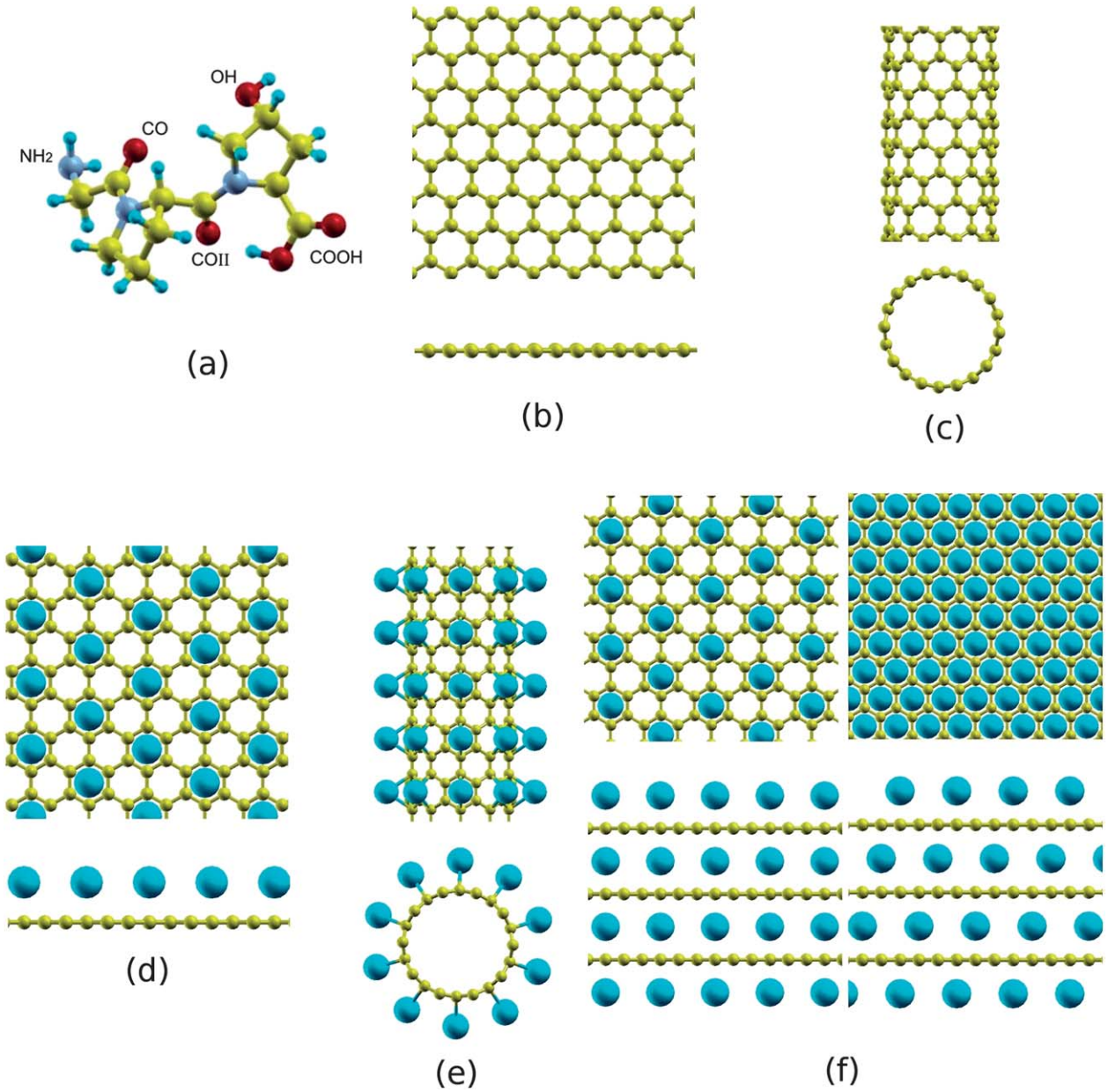

Fig. 1 Sketch of the systems considered: (a) Gly–Pro–Hyp peptide, top and front views of (b) pristine graphene, (c) pristine carbon nanotube, (d) Ca-decorated graphene, (e) Ca-decorated nanotube and (f) α-stacked (left) and αβγ-stacked (right) calcium graphite CaC_6. C, H, O, N and Ca atoms are represented with yellow, blue (small), red, purple and blue (large) spheres, respectively.

atoms), using essentially the same computational approaches as here (see Fig. 1d and e). The size of Ca@CNS systems comprise a total of $63 \leq N \leq 186$ atoms. Armchair (n, n) nanotubes have not been examined in this study because Ca-coatings present a strong thermodynamic tendency for calcium aggregation.[25] Also, we considered bulk calcium graphite, CaC_6, an intriguing graphite intercalate material that becomes a superconductor at low temperatures.[42] This material is composed of alternating planes of Ca and C atoms disposed in triangular and hexagonal lattices, respectively[31,32] (see Fig. 1f). In this compound relative shifts between successive planes of Ca atoms along the out-of-plane graphite direction occur leading to the formation of α (A-…), αβ (A-B-…) and αβγ (A-B-C-…) stacking patterns. For completion, we analyzed both limit α- and αβγ-CaC_6 conformations.

Aimed at exploring the effects of thermal excitations on the stability of peptide–Ca@CNS systems (either in vacuum or aqueous media), we performed *ab initio* molecular dynamics simulations (AIMD) for temperatures $T \geq 300$ K. We used a Verlet-type algorithm and Nosè thermostat for integration of Newton's equations of motion and sampling of the canonical ensembles, respectively. The size of the systems in these AIMD simulations were the same as in the atomic relaxations though, due to the intensive computational cost associated with these calculations, we employed Γ k-point for sampling of the irreducible Brillouin zone. In all the simulations, total times of about 40–70 ps were accessed using a default time step of 1.5 fs (initial AIMD configurations coincide with the equilibrium structures determined in the atomic relaxations). In the simulations

involving water, we considered a total of 39 H_2O molecules at the equilibrium density. It must be noted that, due to the enormous computational cost associated, we did not attempted to perform straightforward water–peptide–Ca@CNS *ab initio* molecular dynamics runs. Rather, we explored the thermal stability and interactions of Ca@CNS in water and estimated the strength of water-mediated peptide–Ca@CNS binding through approximate Gibbs free-energy calculations. Additionally, we present AIMD results for a reduced hybrid system composed of glycine amino acid and Ca@graphene in water.

III. Results and discussion

A. Binding energy, atomic and electronic structure

In Table 1, we report energy results for the binding of small peptides to pristine and Ca-decorated CNS. As it could have been foreseen, peptide–CNS interactions in pristine nanostructures are very weak.[36,43–45] By contrast, very intense peptide–CNS binding is attained in all the cases when the carbon surfaces are decorated with calcium atoms. In particular, we predict $|E_{bind}|$ values of $\sim$1 eV (that is, about a factor of 20 larger than in non-decorated nanostructures) at low and medium calcium concentrations (*e.g.* $X_{Ca} \leq 10\%$) independently of the CNS curvature. Furthermore, peptide–CNS binding becomes increasingly more intense in Ca@graphene as the concentration of calcium atoms is raised. A similar binding trend is observed in *narrow* (6, 0) zig-zag carbon nanotubes (CNT), where the largest binding energy already amounts to 1.8 eV. Unfortunately, we could not infer a general E_{bind} tendency for *wide* CNT (*e.g.* 4 Å $\leq R_{CNT}$) at large Ca concentrations due to the technical difficulties arising in the atomic relaxations (*e.g.* sampling of the corresponding configurational landscapes becomes extremely difficult because of the large size and high energy degeneracy of Ca@CNT systems).

For bulk CaC_6 we considered two situations, one in which the peptide is accommodated on top of a calcium-free carbon surface (referred to as "Pristine" in Table 1), and the other in which the closest neighbours to the molecule are Ca atoms (referred to as "Equilibrium" in Table 1). We observe very weak binding to pristine systems whereas $|E_{bind}|$ values of $\sim$1.7 eV are obtained in calcium-doped surfaces, very much similar to what is found in graphene. We find that the effect of out-of-plane stacking on peptide binding is practically negligible. These results indicate that, depending on the composition of the outermost CaC_6 surfaces, peptide–CaC_6 forces may either be very intense and short-ranged or very weak and long-ranged. This effect opens the possibility of engineering peptide–inorganic interactions by epitaxial growth of CaC_6 films. It is important to note that due to steric effects peptide penetration into bulk CaC_6 is energetically forbidden (*e.g.* the distance between two consecutive carbon planes is $\sim$4.5 Å whereas characteristic peptide lengths are $\sim$8–10 Å).

In Fig. 2–4, we plot the equilibrium peptide–CNS and peptide–Ca@CNS configurations obtained in our geometry optimizations. Since in pristine nanosurfaces peptide–CNS interactions are extremely weak, we restrict the following analysis to Ca-decorated nanohybrids. In flat nanosurfaces (*i.e.* Ca@graphene and CaC_6) we find that the energetically most favoured structures are those in which NH_2, CO and OH peptide atoms (see Section II and Fig. 1a) form bonds with calcium adatoms (bond lengths are $d_{Ca–CO} = 2.3$ and $d_{Ca–OH} = 2.4$ Å in both systems). It is worth noting that oxygen atoms exhibit the largest chemical affinity towards calcium as evidenced by the amount of electronic charge transferred in Ca–N and Ca–O bonds: 0.3 and 0.4 electrons, respectively (according to our CDD analysis). In Ca@CNT we find that only terminal COOH and side-chain COII atoms are involved in optimal peptide binding (with $d_{Ca–COOH} = 2.5$ and $d_{Ca–COII} = 2.4$ Å, almost independently of CNT radius). From a conformational point of view we observe that Ca-decorated CNS are little modified by their interactions with the peptide. The Gly–Pro–Hyp molecule, however, distorts more or less appreciably depending on the system where it binds. Particularly, peptide deformation is more significant in flat Ca-doped surfaces where the distance between neighbouring Ca atoms is the largest. We note that in narrow Ca@CNT the peptide can access the calcium centers just by altering slightly its equilibrium gas-phase geometry (see Fig. 3). Such a conformational peptide–CNT correspondence, dictated by both intrinsic CNT and peptide curvatures, turns out to be energetically advantageous explaining the fact that at high Ca concentrations the strongest binding occurs in the narrowest nanotube (see Table 1).

In order to understand the fundamental mechanisms behind the observed Ca-mediated binding enhancement, we have examined the electronic structure of both peptide–Ca@graphene and peptide–graphene systems. In Fig. 2, we plot the partial density of electronic states (*e.g.* expressed in terms of the s, p and d angular momentum components) as projected into the peptide and graphene units. In comparing the two systems we find that important overlappings between clouds of p-peptide and s, d-metallic electronic states appear in the presence of Ca atoms, within a small energy window surrounding the Fermi level. This strong electronic hybridization of the dp-type induces significant charge rearrangements within the nanohybrids that are in the root of the observed binding enhancement. In particular, when Ca atoms adsorb on graphene (case $X_{Ca} = 16.67\%$, see Fig. 1d) each donates a total of $\sim$0.6 electrons (e^-) to the neighboring carbon atoms. In the presence of the peptide, the metal atoms

Table 1 Gly–Pro–Hyp binding energies (in eV units) expressed as a function of calcium concentration X_{Ca}. Pristine values refer to $X_{Ca} = 0\%$ with the exception of CaC_6 for which they mean peptide binding to the clean graphite surface. Symbol "—" denotes cases in which the equilibrium geometry could not be determined confidently (see text)

Radius	(6, 0) 2.42 Å	(10, 0) 3.96 Å	(12, 0) 4.70 Å	(15, 0) 5.88 Å	Graphene ∞	CaC_6 (α) ∞	CaC_6 (αβγ) ∞
Pristine	−0.017	−0.040	−0.067	−0.063	−0.064	−0.068	−0.055
$X_{Ca} \leq 10\%$	−1.158	−0.846	−1.136	−0.990	−1.176		
$10\% < X_{Ca} \leq 30\%$	−1.842	−0.786	—	—			
Equilibrium	—	—	—	—	−1.655 ($X_{Ca} = 16.67\%$)	−1.662	−1.694

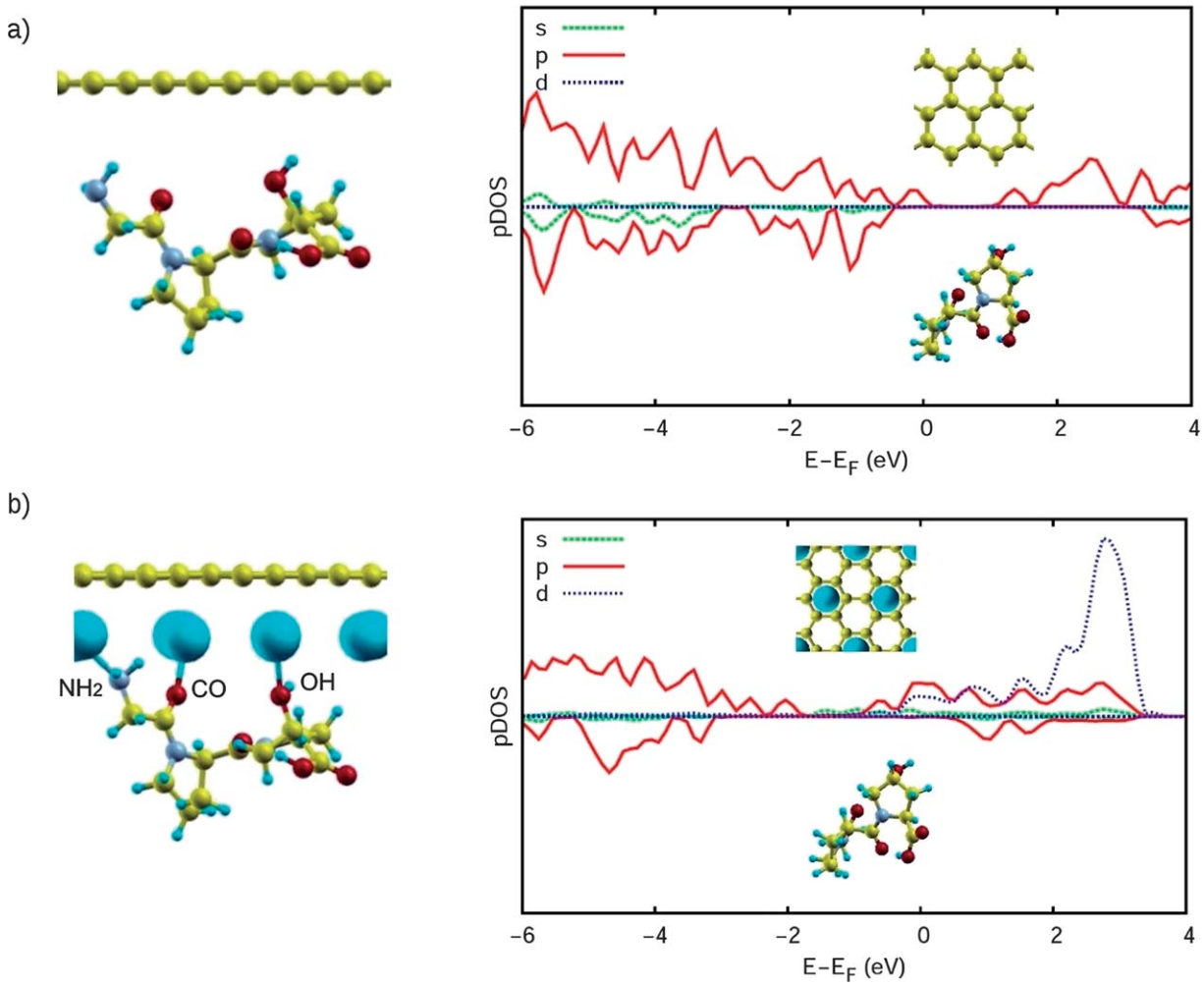

Fig. 2 (a) Geometry optimized peptide–graphene system and corresponding partial density of electronic states. Densities of electronic s, p and d states localized in graphene and the peptide are represented in the upper and lower panel, respectively. (b) Geometry optimized peptide–Ca@graphene system and corresponding partial density of electronic states. Densities of electronic s, p and d states localized in Ca@graphene and the peptide are represented in the upper and lower panel, respectively. The Fermi energy level has been shifted to zero in both cases. C, H, O, N and Ca atoms are represented with yellow, blue (small), red, purple and blue (large) spheres, respectively.

become further positively charged by transferring $\sim 0.4e^-$ to the molecule. These electronic charge transfers induce strong $CNS^{\delta-}$–$Ca^{\delta+}$ and $Ca^{\delta+}$–$peptide^{\delta-}$ Coulomb interactions that result in an effective peptide–graphene attraction. Finally, it is worth mentioning that similar charge rearrangements are very likely to happen in CaC_6 and Ca@CNT systems. Fig. 5, for instance, shows a contour of the electronic-localization function calculated in the peptide–Ca@(10, 0) CNT system (with an excess isosurface value of $0.3e^-$). It is clear that the main areas of electronic density accumulation concentrate around the oxygen (@peptide) and carbon (@CNT) atoms. In addition, CDD analysis predicts charge transfers of $\sim 0.4e^-$ from the Ca dopants to the neutrally charged peptide, exactly as estimated in graphene.

B. Thermal stability of peptide–Ca@CNS systems

In the previous section we have demonstrated that Ca-mediated peptide–CNS interactions are intrinsically selective and very intense. Besides this, a condition that any promising biomaterial must accomplish is to be chemically stable (*i.e.* lacking of any component segregation) at the ambient temperature. Our calculations predict large energy penalties for Ca and Ca–peptide segregation from the peptide–Ca@graphene system in the zero-temperature limit: 1.59 and 6.76 eV, respectively. Nevertheless, these large values do not necessarily guarantee thermal stability of the systems under study since significant kinetic and entropic contributions may be at play. Consequently, explicit simulation of the thermal effects is required.

In Fig. 6, we plot the trajectory of the peptide center of mass (CM) relative to the Ca-doped carbon surface, $\Delta R_{CM}(t) \equiv |R_{CM}(\text{peptide}) - R_{CM}(\text{Ca@Gr})|(t)$, expressed as a function of time and temperature. After an initial interval of $\sim$5 ps the difference between the peptide and Ca@graphene CM remains practically constant ($T = 300$ K) so indicating stable peptide binding (in fact, if the peptide detached from graphene the corresponding $\Delta R_{CM}(t)$ function would display wide oscillations). In order to unmask possible system instabilities triggered by

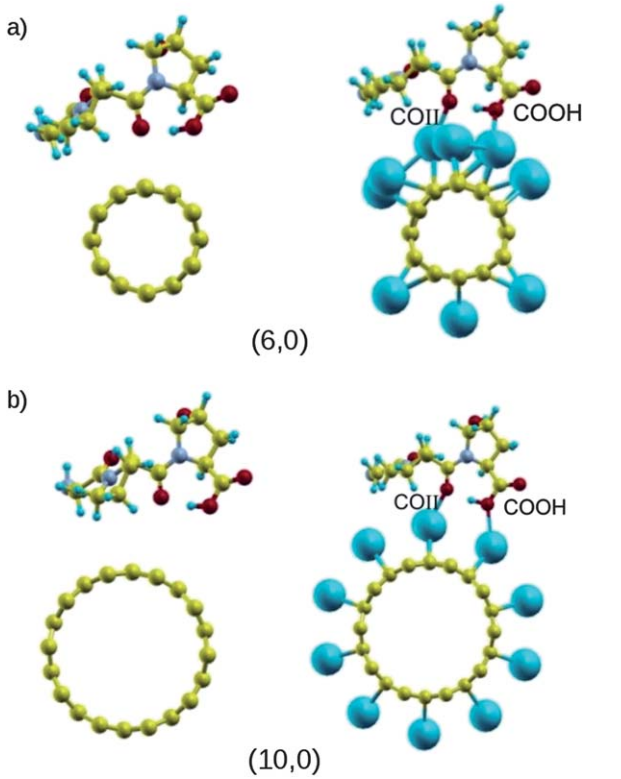

Fig. 3 (a) Front views of the geometry optimized peptide–(6, 0) CNT and peptide–Ca@(6, 0) CNT systems. (b) Front views of the geometry optimized peptide–(10, 0) CNT and peptide–Ca@(10, 0) CNT systems. The atomic color code is the same as that used in previous figures.

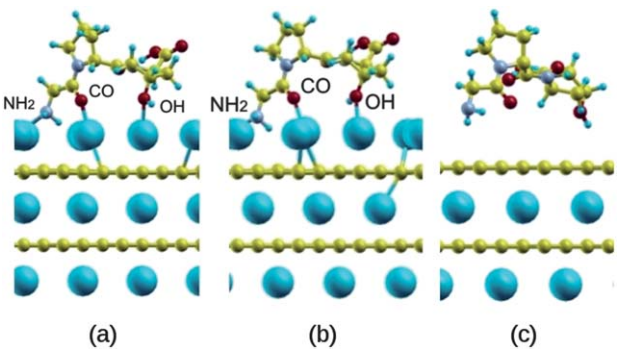

Fig. 4 Optimized peptide–CaC_6 geometries obtained for (a) α, (b) αβγ and (c) pristine αβγ calcium graphite stacking. The atomic color code is the same as that used in previous figures.

large atomic displacements, we raised the temperature of the system up to 450 K. However, no significant $\Delta R_{CM}(t)$ differences with respect to the $T = 300$ K case are appreciated.

Aimed at getting a more detailed description of temperature effects in peptide–Ca@CNS composites, we monitored the time evolution of the projection of the peptide CM over graphene (arbitrarily denoted as $x - y$), $R_{CM,xy}(t)$. This quantity may be useful for detecting possible peptide diffusion which, in the case of involving a too small scale, could have escaped from our previous $\Delta R_{CM}(t)$ analysis. As one can see in Fig. 6, $R_{CM,xy}(t)$ varies just slightly within the first picoseconds of the simulation and remains roughly constant around a value of 2 Å at any

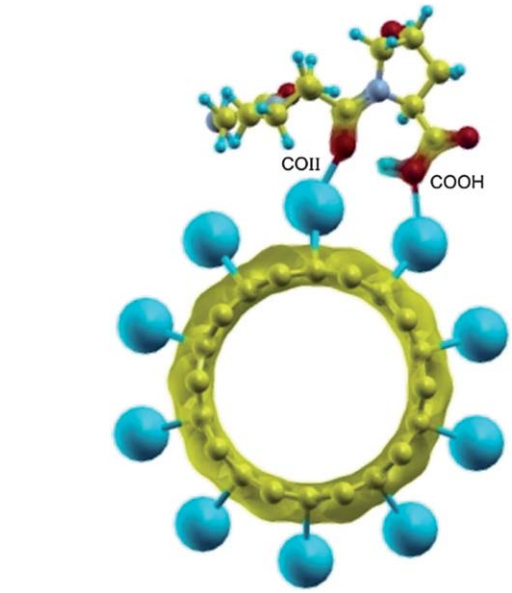

Fig. 5 Contour of the electronic-localization function obtained in the equilibrium peptide–Ca@(10, 0) CNT system. Areas of electronic density accumulation relative to the pristine case are denoted with blur texture. The atomic color code is the same as that used in previous figures.

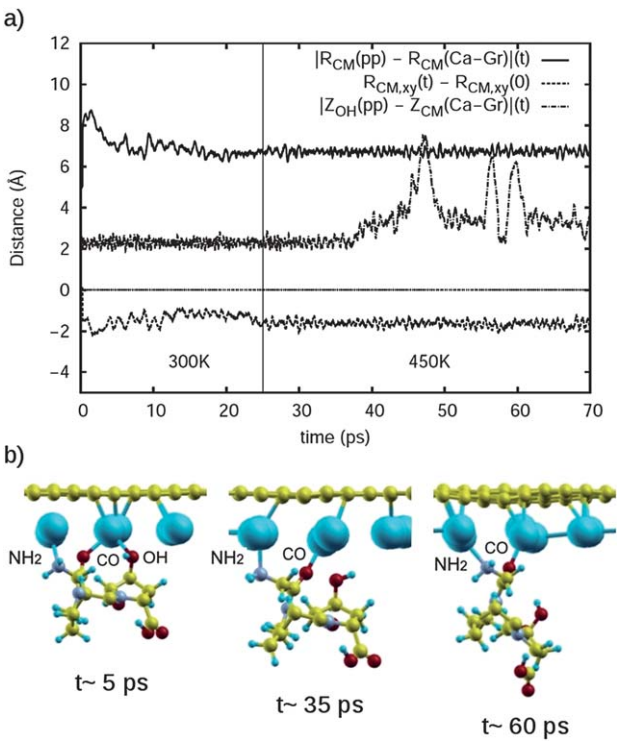

Fig. 6 (a) *Ab initio* molecular dynamics results obtained in peptide–Ca@graphene at $300 \leq T \leq 450$ K: trajectory of the peptide CM relative to the calcium-decorated carbon surface and its projection over graphene (arbitrarily defined as $x - y$) expressed as a function of time. The distance of the peptide OH atom to the carbon plane is also shown. (b) "Ball–stick" representation of atomic configurations generated in the dynamical simulations. The atomic color code is the same as that used in previous figures.

subsequent moment. In fact, this result corroborates our previous conclusion. Finally, we generated "ball–stick" representations rendering the sets of atomic configurations produced in the AIMD runs. In doing this we realized that NH_2, CO and OH atoms alternate in forming bonds with the calcium adatoms so inducing oscillations of the peptide around its center of mass. This is clearly shown in Fig. 6 where we monitor the distance of the OH peptide atom to graphene as a function of time.

In summary, our results show that thermal stability of peptide–Ca@CNS nanohybrids is very robust and organic mass transport over Ca-decorated graphene very improbable. It follows that tight peptide immobilization on CNS by covalent Ca-based functionalization is in principle attainable.

C. Thermal stability of Ca@CNS in water

In order to achieve effective conjugation with biocomponents of interest (*e.g.* proteins and molecules), promising biomaterials and molecular transporters must be non-degradable and highly soluble in physiological solutions.[12,46–49] Pristine carbon nanostructures, however, are highly hydrophobic. Moreover, CNS interact through attractive π–π stacking forces so that when immersed in water they tend to cluster forming micelles in order to minimize their total energy.

A clear manifestation of the intrinsic hydrophobicity of CNS is shown in Fig. 7, where we plot the density of H_2O molecules along the out-of-plane direction of graphene obtained at $T =$ 300 K. It is observed that in the region close to the carbon surface (*i.e.* $z \leq 5$ Å, where z represents the minimum distance between a H_2O molecule and graphene) the presence of water molecules is practically vanishing. This appreciation, however, is in stark contrast with results obtained in Ca@graphene where a large and narrow (*i.e.* ~1.2 Å wide) density peak appears at $z \sim 4$ Å. Since Ca adatoms accommodate at a distance of $z = 2.4$–2.8 Å from graphene, a large portion of water molecules is already localized very close to the metal coating. In fact, we realized *via* examination of the AIMD configurations that H_2O molecules get actually trapped into the Ca interstitials. This is a direct consequence of the natural reactivity of calcium in water, which in the present context has an important and positive repercussion: to significantly reduce graphene's hydrophobicity.

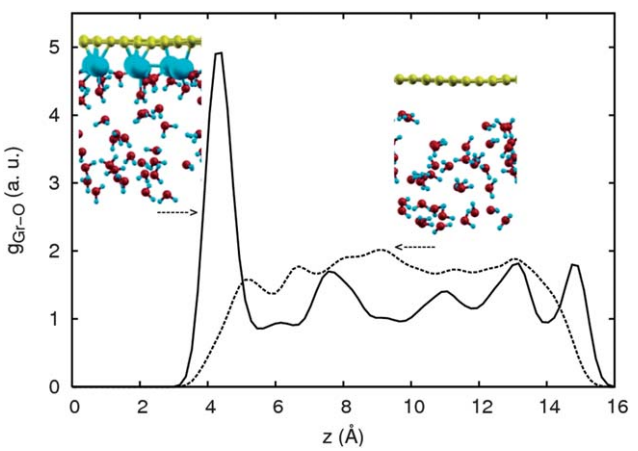

Fig. 7 Density profile of water molecules along the out-of-plane direction of graphene (defined as z) in the presence (solid line) and absence (dashed line) of Ca adatoms ($T = 300$ K). Results were obtained by averaging the atomic positions over a 40 ps long *ab initio* molecular dynamics simulation. The atomic color code is the same as that used in previous figures.

Aimed at getting further insight into the effects of water molecules on the thermal stability of Ca@graphene, we analyzed the radial Ca–Ca distribution function and diffusion of the CM of the Ca-coating at $T = 300$ K (see Fig. 8). We define the radial Ca–Ca distribution function, g_{Ca-Ca}, as:

$$g_{Ca-Ca}(r) = \frac{1}{N_{Ca}(N_{Ca}-1)} \sum_{i \neq j}^{N_{Ca}} \langle \delta(|\boldsymbol{R}_{ij}| - r) \rangle, \qquad (2)$$

where $\boldsymbol{R}_{ij}$ stands for the position vector connecting the centers of atoms i and j, N_{Ca} the total number of atoms, and $\langle \ldots \rangle$ the average performed in the canonical (N, V, T) ensemble. As seen in Fig. 8, the $g_{Ca-Ca}(r)$ profile calculated at room-temperature exhibits two main peaks centered at the same first- and second-nearest neighbour positions as obtained at $T = 0$ K (*i.e.* the perfect commensurate lattice case). In the former case, g_{Ca-Ca} peaks are actually broadened by the effect of atomic fluctuations, however no evidence for calcium segregation can be inferred from our results (*i.e.* $\lim r \rightarrow \infty g_{Ca-Ca}(r) \neq ct.$). The same conclusion is reached after inspection of the time evolution of the CM calcium coating, which remains roughly constant along the whole simulation (see Fig. 9).

Interestingly, we identified the formation of H_2 molecules in water at ~10 ps past the start of the simulation (see Fig. 9b). Since our simulations are performed under equilibrium thermodynamic conditions, the appearance of molecular hydrogen must signal spontaneous water dissociation processes of the type:

$$Ca + 2H_2O \rightarrow Ca(OH)_2 + H_2$$

occurring at the water–graphene interface. In Fig. 10, we show details of the first solvation shell of water molecules stabilized over Ca@graphene. Certainly, few H_2O molecules have dissociated as shown by the presence of hydroxide ions (*e.g.* OH^-) adsorbed on top of calcium atoms. The pursuit of these dissociations is to create new three- and two-fold coordinated Ca–OH bonds that

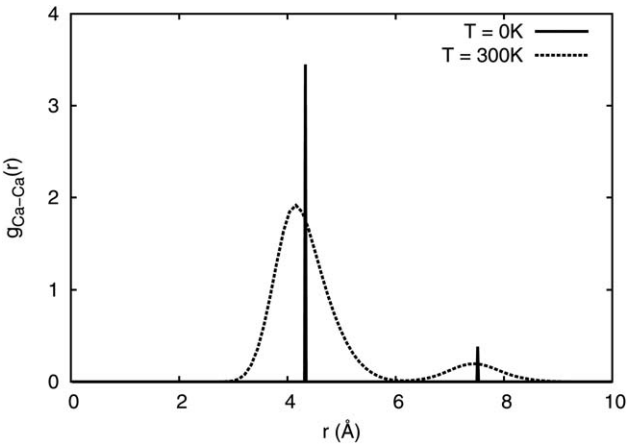

Fig. 8 Calculated Ca–Ca radial distribution function in Ca@graphene immersed in water as a function of temperature. Finite-T results were obtained by averaging the atomic positions over a 40 ps long *ab initio* molecular dynamics simulation.

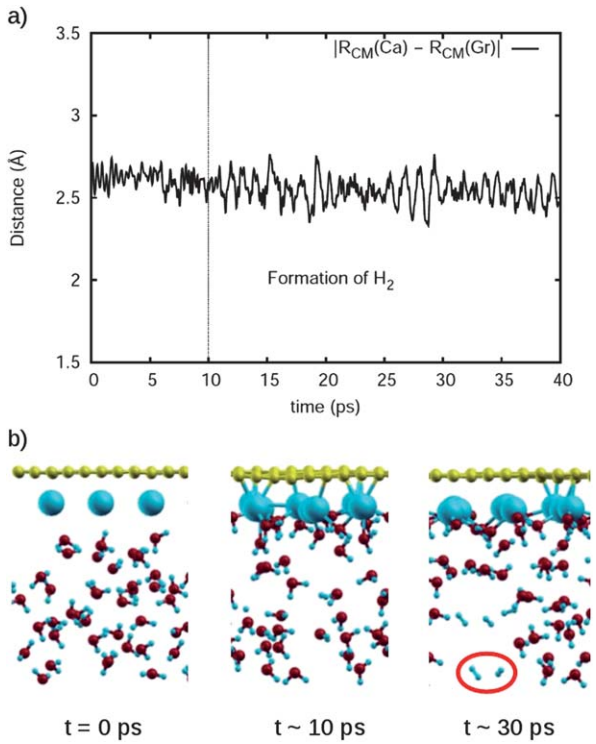

Fig. 9 (a) CM trajectory of the calcium coating with respect to graphene immersed in water ($T = 300$ K); molecular hydrogen is formed as a result of water dissociation processes in the metal surface. (b) "Ball–stick" representation of atomic configurations generated in the dynamical simulations; hydrogen molecules are highlighted with a red ellipse. The atomic color code is the same as that used in previous figures.

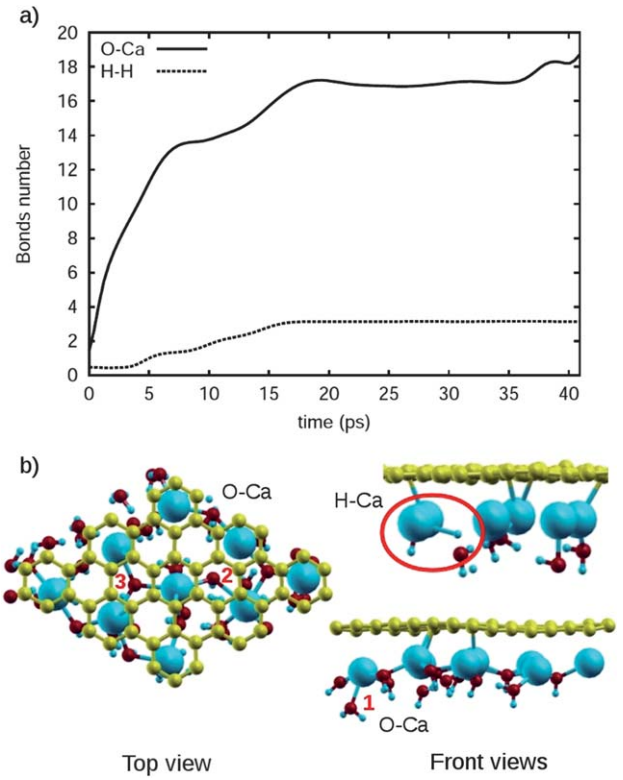

Fig. 10 (a) Dissociation of H_2O molecules and consequent formation of O–Ca and H–H bonds in Ca@graphene immersed in water ($T = 300$ K). (b) Plot of the newly formed three-fold (3), two-fold (2) and single (1) coordinated O–Ca and H–Ca bonds. Water molecules far from graphene have been removed in order to improve visualization. The atomic color code is the same as that used in previous figures.

are energetically more favorable than H–OH water bonds (as we will show in the next section). As a result of these processes, neutral H atoms hop over graphene by forming transient bonds with calcium atoms (see Fig. 10). Eventually, two hydrogen hopping atoms meet and recombine forming a H_2 molecule that dives into the solvent. It is worth noting that water dissociation reactions in Ca-coated graphene seem to saturate quite promptly, approximately after a total of $\frac{2}{3}N_{Ca}$ water molecules is reduced. We estimated this saturation threshold by monitoring the total number of H–H and Ca–O bonds formed along the simulation (see Fig. 10a, numbers of bonds were determined according to the atomic geometric criteria $|\boldsymbol{R}_{H-H}| \leq 0.85$ Å and $|\boldsymbol{R}_{Ca-O}| \leq 2.50$ Å). Specifically, we found that the stationary number of H_2 molecules was three so implying that a total of six H_2O molecules (that is, two thirds the number of Ca atoms in our simulation cell) had dissociated. It is important to note that calcium–oxygen coordination may actually swing between three- and two-fold, and that water molecules which do not dissociate can also interact with the metal atoms forming single coordinated Ca–O bonds (see Fig. 10b); consequently, the total number of Ca–O bonds fluctuates during all the simulations.

D. Peptide–Ca@CNS *versus* H_2O–Ca@CNS selectivity

In the previous section we have shown that Ca-decorated carbon nanostructures are very likely to be miscible and non-degradable in water. Nevertheless the unveiled H_2O–Ca@graphene interactions might pose a serious competition to peptide binding so hampering effective realization of peptide–Ca@CNS composites in aqueous media.

In order to assess the peptide *versus* H_2O selectivity of Ca@CNS at room temperature, we estimated the Gibbs free energy balance, ΔG, of the following three-steps reaction sketched in Fig. 11. Initially, one free H_2O molecule binds to Ca@graphene losing one H atom (Step 1); next, one proton from a peptide carboxyl group is transferred to the hydroxide ion still immobilized on graphene (Step 2); finally, the peptide binds to the metal center and liberates one H_2O molecule (Step 3). Step 1 represents water dissociation processes explained in the previous section (thus presumably the corresponding partial energy balance ΔG_1 will be negative) while Steps 2 and 3 account for peptide against H_2O binding competitions (that is, peptide binding will be preferred over H_2O–Ca@CNS binding if $\Delta G_{2\rightarrow 3} \leq 0$ whereas the opposite will be preferred if $0 \leq \Delta G_{2\rightarrow 3}$). In our calculations, we disregarded H_2 and H_2O entropic contributions to ΔG and assumed Step 2 to be correctly described as a standard acid–base reaction (*e.g.* $\Delta G_{acid-base} = -RT \ln K_{eq.}$, where $K_{eq.} = K_a(RCOOH)/K_a(H_2O)$ with $K_a(RCOOH) = 10^{-4.5}$ and $K_a(H_2O) = 10^{-15.7}$). We found that the total Gibbs free-energy reaction balance ΔG is -4.3 eV, with $\Delta G_1 = -2.2$ eV (as expected) and $\Delta G_{2\rightarrow 3} = -2.1$ eV. This result indicates that, despite H_2O molecules strongly interacting with calcium atoms, peptide-Ca@CNS binding is favored.

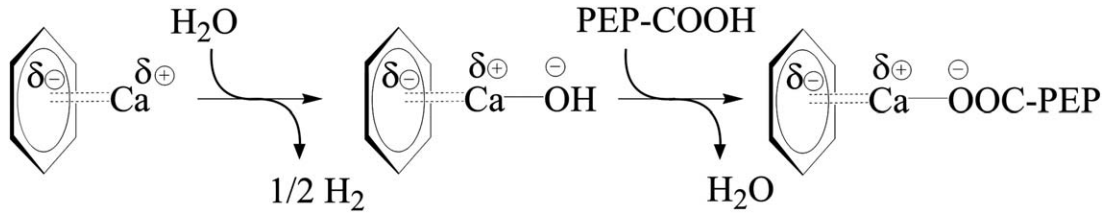

Fig. 11 Sketch of the proposed three-steps reaction for assessment of the peptide against H_2O binding selectivity of Ca@graphene. Partial reaction energy balances, calcium oxidation states and graphene–peptide charge states are indicated in the figure. Graphene is represented by a 6-atom carbon ring.

Finally, we simulated a hybrid glycine–Ca@graphene system immersed in water ($T = 300$ K). The main goal of this simulation was to test, at least at a qualitative level, our predictions above. Results are enclosed in Fig. 12 where we plot the CM difference between the amino acid and Ca@graphene along the out-of-plane direction and as a function of time. At $t = 0$, the amino acid is placed at a distance of approximately half the length of the simulation cell from graphene (*e.g.* ~8 Å). Within the first simulated picoseconds we observe that glycine transitions from a neutral to a zwitterionic state in which the carboxyl termination gets deprotonated by the amine group (*e.g.* $NH_2CH_2COOH \rightarrow NH_3^+CH_2COO^-$). As time evolves, $\Delta Z_{CM}(t) \equiv Z_{CM}(\text{Gly}) - Z_{CM}(\text{Ca@graphene})(t)$ steadily decreases until reaching a small average value of ~4.2 Å. From t ~20 ps on, we observe that the amino acid carboxyl termination keeps close to and orientated towards the carbon surface most of the time (see evolution of the COOH group position in Fig. 12). Eventually, glycine binds to the calcium coating creating a new Ca–O bond (see Fig. 12b). These outcomes show that glycine is effectively attracted towards graphene despite the screening caused by the presence of H_2O molecules. We can conclude, therefore, that room-temperature trends observed in a small amino acid–Ca@CNS system are consistent with our predictions for robust water-mediated peptide–Ca@CNS binding.

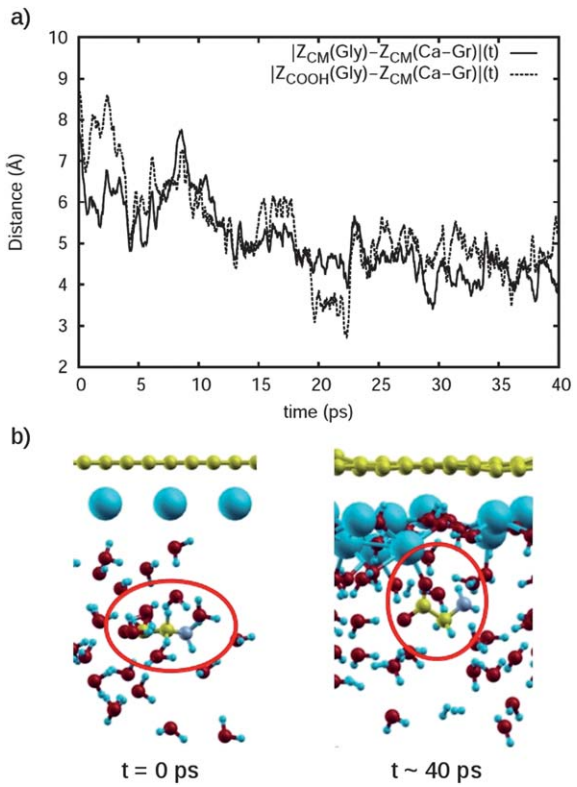

Fig. 12 (a) Out-of-plane component of the glycine center of mass and COOH oxygen position relative to Ca@graphene immersed in water ($T =$ 300 K). (b) "Ball–stick" representation of atomic configurations generated in the AIMD simulations; amino acid location is highlighted with a red ellipse. The atomic color code is the same as that used in previous figures.

IV. Conclusions

Based on density functional theory simulations, we foresee an efficient and technically simple covalent functionalization strategy for precise immobilization of peptides on the surface of carbon nanostructures immersed in water. This strategy consists of straightforward decoration of CNS surfaces with calcium atoms and represents a series of improvements with respect to customary covalent oxidizing CNS approaches. First, strong and highly selective peptide–Ca@CNS forces are accomplished without inflicting structural damage on the carbon nanosurfaces. Second, CNS solubility in aqueous media is significantly enhanced as a result of the attractive forces between H_2O molecules and calcium atoms thus no additional functionalization for CNS water miscibility is required. In the light of our results, Ca-decorated CNS emerge as a promising class of inorganic substrates for the creation of artificial biomimetic surfaces and molecular transporters. Seemingly, CaC_6, a bulk graphitic material of identical chemical composition, can be regarded as a potential substrate for medical implant applications (*i.e.* orthopaedic implant coatings in alternative to commercially pure titanium and hydroxyapatite) due to its favourable reactive and mechanical (*e.g.* tensile strength, fracture toughness and resistance, not analyzed in this study) properties. In view of present great interest in drug delivery and biomaterials applications, we encourage experimental searches for the synthesis and assessment of the biotechnological potential of Ca-based carbon nanomaterials.

Acknowledgements

The authors thankfully acknowledge the computer resources, technical expertise and assistance provided by the Barcelona Supercomputing Center-Centro Nacional de Supercomputación (BSC-CNS). This work was carried out under the

HPC-EUROPA2 project (project number: 228398) with the support of the European Commission Capacities Area – Research Infrastructures Initiative. We also acknowledge support by MICINN-Spain (grants no. MAT2010-18113, CSD2007-00041, and FIS2008-03845) and Generalitat de Catalunya (GENCAT, grant 2109SGR-1309).

References

1 R. Saito, G. Dresselhaus and M. S. Dresselhaus, *Physical Properties of Carbon Nanotubes*, MS World Scientific, 1998.
2 A. H. Castro Neto, F. Guinea, N. M. R. Peres, K. S. Novoselov and A. K. Geim, *Rev. Mod. Phys.*, 2009, **81**, 109.
3 I. Willner, *Science*, 2002, **298**, 2407.
4 K. A. Willams, P. T. M. Veenhuizen, B. G. de la Torre, R. Eritja and C. Dekker, *Nature*, 2002, **420**, 761.
5 S. C. Tsang, Z. J. Guo, Y. K. Chen, M. L. Green, H. A. Hill, T. W. Hambley and P. J. Sadler, *Angew. Chem., Int. Ed. Engl.*, 1997, **36**, 2198.
6 C. V. Nguyen, L. Delzeit, A. M. Cassell, J. Li, J. Han and M. Meyyappan, *Nano Lett.*, 2002, **2**, 1079.
7 H. J. Dai, *Acc. Chem. Res.*, 2002, **35**, 1035.
8 R. H. Baughman, A. A. Zakhidov and W. A. de Heer, *Science*, 2002, **297**, 787.
9 H. P. Yiu and P. A. Wright, *J. Mater. Chem.*, 2005, **15**, 3690.
10 E. Ruiz-Hitzky, M. Darder, P. Aranda and K. Ariga, *Adv. Mater.*, 2010, **22**, 323.
11 B. Dunn and J. I. Zink, *Acc. Chem. Res.*, 2007, **40**, 747.
12 W. Yang, P. Thordarson, J. J. Gooding, S. P. Ringer and F. Braet, *Nanotechnology*, 2007, **18**, 412001.
13 S. C. Tsang, J. J. Davis, M. L. H. Green, H. A. O. Hill, Y. C. Leung and P. J. Sadler, *Chem. Commun.*, 1995, 1803.
14 R. J. Chen, Y. Zhang, D. Wang and H. Dai, *J. Am. Chem. Soc.*, 2001, **123**, 3838.
15 B. R. Azamian, J. J. Davis, K. S. Coleman, C. B. Bagshaw and M. L. H. Green, *J. Am. Chem. Soc.*, 2002, **124**, 12664.
16 W. Huang, S. Taylor, K. Fu, Y. Lin, D. Zhang, T. W. Hanks, A. M. Rao and Y. P. Sun, *Nano Lett.*, 2002, **2**, 311.
17 K. Besteman, J. O. Lee, F. G. M. Wiertz, H. A. Heering and C. Dekker, *Nano Lett.*, 2003, **3**, 727.
18 M. Holzinger, O. Vostrowsky, A. Hirsch, F. Hennrich, M. Kappes, R. Weiss and F. Jellen, *Angew. Chem., Int. Ed.*, 2001, **40**, 4002.
19 A. Hirsch, *Angew. Chem., Int. Ed.*, 2002, **41**, 1853.
20 K. Jiang, L. S. Schadler, R. W. Siegel, X. Zhang, H. Zhang and M. Terrones, *J. Mater. Chem.*, 2004, **14**, 37.
21 J. L. Bahr and J. M. Tour, *J. Mater. Chem.*, 2002, **12**, 1952.
22 U. Bangert, A. Bleloch, M. H. Gass, A. Seepujak and J. van den Berg, *Phys. Rev. B: Condens. Matter Mater. Phys.*, 2010, **81**, 245423.
23 C. Pagura, S. Barison, C. Mortalo, N. Comisso and M. Schiavon, *Nanosci. Nanotechnol. Lett.*, 2012, **4**, 160.
24 N. Almora-Barrios and N. H. de Leeuw, *CrystEngComm*, 2010, **12**, 960.
25 C. Cazorla, S. A. Shevlin and Z. X. Guo, *Phys. Rev. B: Condens. Matter Mater. Phys.*, 2010, **82**, 155454.
26 M. Yoon, S. Yang, C. Hicke, E. Wang, D. Geohegan and Z. Zhang, *Phys. Rev. Lett.*, 2008, **100**, 206806.
27 X. Yang, R. Q. Zhang and J. Ni, *Phys. Rev. B: Condens. Matter Mater. Phys.*, 2009, **79**, 075431.
28 C. Cazorla, S. A. Shevlin and Z. X. Guo, *J. Phys. Chem. C*, 2011, **115**, 10990.
29 C. Ataca, E. Artük and S. Ciraci, *Phys. Rev. B: Condens. Matter Mater. Phys.*, 2009, **79**, 041406(R).
30 S.-G. Wang, X.-Y. Liao, D.-B. Cao, C.-F. Huo, Y.-W. Li, J. Wang and H. Jiao, *J. Phys. Chem. C*, 2007, **111**, 16934.
31 M. S. Dresselhaus and G. Dresselhaus, *Adv. Phys.*, 2002, **51**, 1.
32 N. Emery, C. Herold and P. Lagrange, *J. Solid State Chem.*, 2005, **178**, 2947.
33 P. E. Blöchl, *Phys. Rev. B: Condens. Matter Mater. Phys.*, 1994, **50**, 17953.
34 G. Kresse and J. Furthmüller, *Phys. Rev. B: Condens. Matter Mater. Phys.*, 1996, **54**, 11169.
35 J. P. Perdew, K. Burke and M. Ernzerhof, *Phys. Rev. Lett.*, 1996, **77**, 3865.
36 C. Cazorla, *Thin Solid Films*, 2010, **518**, 6951.
37 C. Cazorla, D. Errandonea and E. Sola, *Phys. Rev. B: Condens. Matter Mater. Phys.*, 2009, **80**, 064105.
38 H. J. Monkhorst and J. D. Pack, *Phys. Rev. B: Solid State*, 1976, **13**, 5188.
39 L. Bengtsson, *Phys. Rev. B: Condens. Matter Mater. Phys.*, 1999, **59**, 12301.
40 R. F. W. Bader, in *Atoms in Molecules. A Quantum Theory*, Oxford University Press, New York, 1990.
41 G. Henkelman, A. Arnaldsson and H. Johnsson, *Comput. Mater. Sci.*, 2006, **36**, 354.
42 M. Calandra and F. Mauri, *Phys. Rev. Lett.*, 2005, **95**, 237002.
43 T. Roman, W. A. Dinyo, H. Nakanishi and H. Kasai, *Thin Solid Films*, 2006, **509**, 218.
44 W. Qin, X. Li, W.-W. Bian, X.-J. Fan and J.-Y. Qi, *Biomaterials*, 2010, **31**, 1007.
45 C. Rajesh, C. Majumder, H. Mizuseki and Y. Kawazoe, *J. Chem. Phys.*, 2009, **130**, 124911.
46 D. Pantarotto, C. D. Partidos, R. Graff, J. Hoebeke, J. P. Briand, M. Prato and A. Bianco, *J. Am. Chem. Soc.*, 2003, **125**, 6160.
47 M. Sano, A. Kamino, J. Okamura and S. Shinkai, *Langmuir*, 2001, **17**, 5125.
48 F. Pompeo and D. E. Resasco, *Nano Lett.*, 2002, **2**, 369.
49 W. Zhao, C. Song and P. E. Pehrsson, *J. Am. Chem. Soc.*, 2002, **124**, 12418.